Guo Yunlong (Orcid ID: 0000-0002-4490-2140)

Segmental and interfacial dynamics quantitatively determine ion transport in solid polymer composite electrolytes

Yage Huang[1], *Xintong Mei*[1], *and Yunlong Guo*[1,*]

[1]*University of Michigan – Shanghai Jiao Tong University Joint Institute, Shanghai Jiao Tong University, Shanghai 200240, China.*

E-mail: yunlong.guo@sjtu.edu.cn

Abstract

Solid polymer-ceramic composite electrolytes (PCEs) have attracted vast attention for developing solid-state batteries. However, slow ion transport at ambient temperature impedes unlocking their potential. Improving ionic conductivity of PCEs remains a major challenge because ion transport mechanism in complicated composites is not currently available. This article, for the first time, demonstrates that segmental motion and interfacial polarization are directly coupled, both quantitively determine ion transport in PCEs. Adding small-molecule additives enhances ionic conductivity in PCEs, by increasing concentration of ions participating in transport and by equally accelerating segmental motion and interfacial dynamics. Accordingly, an ionic conductivity achieves 1.3×10^{-3} S/cm at 30 °C, simultaneously with high mechanical strength and toughness (solid and flexible, shear modulus $G' > 1$ MPa). The results may shed a light for better analysis and improved design of solid composite electrolytes, toward meeting material demands for next-generation electrochemical energy storage.

This is the author manuscript accepted for publication and has undergone full peer review but has not been through the copyediting, typesetting, pagination and proofreading process, which may lead to differences between this version and the Version of Record. Please cite this article as doi: 10.1002/app.52143

1. Introduction

The development of solid-state electrolytes (SSEs) is crucial to meet the challenge of material demands in next-generation secondary batteries where electrodes and electrolytes are widely recognized to be solid materials.[1] To achieve an exceptional electrochemical performance, structural stability, and battery safety, typical cutting-edge SSEs integrate merits from multiple materials, including fast ion transport in ceramics and mechanical flexibility in polymers.[2] Consequently, polymer-ceramic composite electrolytes (PCEs) attract tremendous scientific and technological interest.[3-7] For instance, a great deal of attention has been paid to composites fabricated by dispersing garnet-type particles in poly(ethylene oxide) (PEO) host, while keeping their traits of low cost and suitable mechanical toughness.[8] Despite recent progress in such PCEs, their low ionic conductivity (~10^{-4} S/cm) at ambient temperature remains a formidable obstacle.

Mechanisms of ion transfer in solid composites are complicated. Microstructures and phases, together with physical and chemical properties of various constituents significantly affect ionic conductivity and ion-transport pathways. In a polymer matrix, ionic motion is strongly coupled with segmental dynamics of the chain molecules.[9-11] Ion transport is contributed from both sub-diffusive motion along chain segments and intersegmental hopping.[12] To achieve a competitive ionic conductivity, addition of ceramic particles benefits polymer electrolytes by reducing crystallinity, although the original intention for introducing such fillers is to exploit their superiority in ion transport. It has been demonstrated that small particles with relatively low fractions enhance ion transport, which is in line with percolation simulations.[13, 14] Nevertheless, insufficient loading often makes limited continuous pathways along interconnected ceramic particles, whereas overabundant fillers usually agglomerate and result in loss of interphase volume hence obstructing formation of percolating network, known as the blocking effect.[15] Ion transport through polymer domain is indispensable under such scenario.

Following the strategy of building continuous freeway for Li^+, recent works using oriented nanowires showed a considerable increase of ionic conductivity, and exhibited ion pathways on the surface of nanowires.[16-18] Moreover, the preference of ion transport along interface rather than entering interior of ceramics, was further proved by the high conductivity under large volume fraction of interfaces.[19] In addition, new twists ranging from copolymerization,[20-22] chain network,[23, 24] polymer blend,[25] and nano-porous structure,[19, 26] to ionic side group[27] and plasticizer, [28, 29] bring promising improvements. Releasing the potential of solid composite electrolytes requires mastering mechanism of ion transport in such materials. However, in multiphase PCEs, models quantitatively demonstrating ion transport through polymer domains and surface charge layers are still unavailable.

This study establishes quantitative coupling equations, for the first time, between ion transport and multiple micro-dynamic processes in PCEs, that is, the EIS properties can be fully described and predicted by dielectric relaxation spectroscopy (DRS) dynamic analysis. Li^+ transfer rate strongly depends on relaxation time and dielectric strength in polymer chains and at polymer-ceramic interfaces. Adding plasticizer raises ionic conductivity (> 10^{-3} S/cm at 30 °C) by equally accelerating segmental and interfacial dynamic processes. With this information, the ion transfer mechanism is deeply understood, which offers valuable strategies for increasing ambient σ_{dc} in PCEs.

Our samples consist of $Li_{6.4}La_3Zr_{1.4}Ta_{0.6}O_{12}$ (LLZTO) or SiO_2 particles, uniformly dispersed in PEO host, with various weight loadings. $LiClO_4$ salt is added to the composite with a molar ratio to EO of 1:18. The samples are accordingly labeled by PEO_{18}-$LiClO_4$-*x* wt% LLZTO (or SiO_2) where the labels indicate indicate the particle diameter. In other cases, certain amount of plasticizer diethylene glycol dimethyl ether (DEGDME) was introduced into the sample, to probe the origin of ion transport enhancement by tuning micro-dynamics.

2. Results and Discussion

2.1 Correlation between local dynamics and electrochemical impedance response

Figure 1 correlates the microscopic dynamic processes with the electrochemical property in a representative PCE. The frequency spectra of dielectric permittivity (Figure 1a) can be divided into three regions, which are dominated by segmental relaxation (α and α_2 process), Maxwell–Wagner–Sillars (MWS) interfacial polarization, and electrode polarization (EP), respectively. Boundaries of these regions are determined from the 2nd-order derivative of ε'_r, as interpreted in *Supporting Information*. At $10^3 - 10^4$ Hz, a frequency zone led by the α_2 relaxation and MWS process, ε''_r shows a linear dependence with a rate of -0.94 (inset in Figure 1a), indicating the ionic transport. Correspondingly, the ionic conductivity (σ_{dc}) is determined from in-phase part of $\sigma'(\omega) = \varepsilon''_r(\omega)\varepsilon_0\omega$, where ε_0 is the permittivity of vacuum. The permittivity response is decomposed into several key contributors, as demonstrated in Figure 1b. From the trend of gradual leveling off of ε''_r at high frequencies, we detected two α processes, which are speculated to be originated from the relative fast (α) and slow (α_2) modes of segmental motion under different levels of confinement of amorphous phases among LLZTO particles and PEO crystal phases.

Remarkably, intensities of dynamic processes show a inverse relationship with the frequency. This trend reflects the large length scale and greater number of ions getting involved in the individual dynamic processes from segmental motion, to MWS polarization, and to EP.

To examine the influence of segmental relaxation and interfacial polarization on ionic conductivity in solid PCEs, electrochemical impedance spectrum (EIS) was measured with two stainless steel blocking electrodes for various samples. In line with the permittivity results, EIS exhibits three major regions with approximately identical boundaries, as marked in Figure 1c. From high to low frequencies, the regions show a semicircle, a slightly curved line, and a spike, respectively, representing the responses from local dynamics in amorphous phase of PEO, PEO-LLZTO dielectric boundary layers, and electrolyte-electrode interfaces. This is further confirmed by reproducing the EIS profile using Nyquist characteristics of segmental

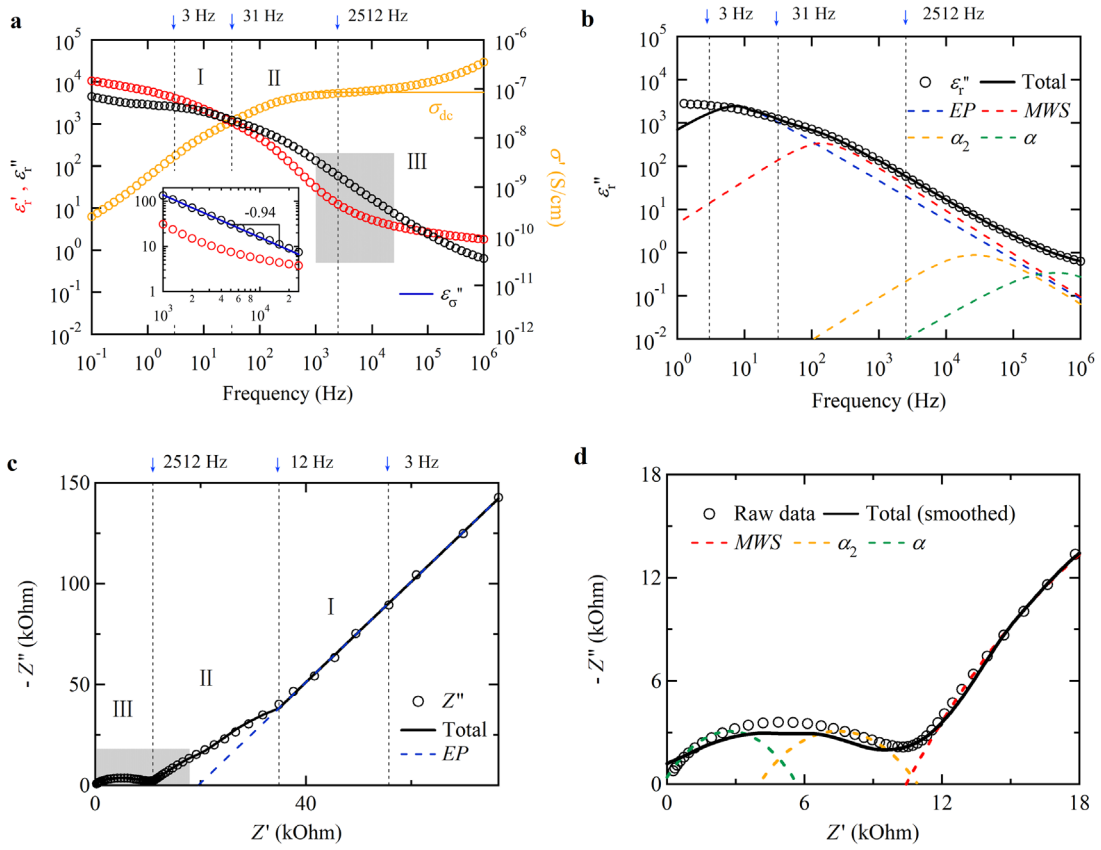

Figure 1. Representative dielectric frequency spectra and Nyquist plot of ac-impedance measurements. (a) Dielectric relaxation spectra. The inset shows an ionic conduction with a slope of nearly -1 in the grey area. **(b)** Decomposition of the loss dielectric permittivity into several sub-processes. The dash curves represent processes described by Equation (7) and (8). **(c)** The corresponding Nyquist plot under identical condition. Open circles represent raw data from EIS measurements, while the solid curve represents the sum of response from dynamic processes. **(d)** Details of the grey area in (c). Ⅰ, Ⅱ and Ⅲ in (a) and (c) represent regions dominated by EP, MWS and segmental relaxations, respectively. Data are measured at 10 ℃, for the sample of PEO_{18}-$LiClO_4$ with dispersed 100 nm-SiO_2 particles at 10 wt%.

relaxations , MWS polarization, and EP.[30] The dash curves in Figure 1c and 1d are computed from the results in Figure 1b according to $\varepsilon_r^*(\omega) = 1/(i\omega Z^*(\omega)C_0\varepsilon_0)$, where C_0 is the capacitance of the empty capacitor. The sum of impedance from these dynamic processes (black curve, slightly smoothed) matches the data well. These results suggest a direct and strong correlation between micro-dynamics and EIS results exists. That is, the electrochemical response can be derived from, and controlled by dynamic processes in which ion transport gets involved, without conducting EIS measurements.

2.2 Modeling ionic conductivity

EIS measurements were conducted on our PCE samples containing inert (SiO_2) or superior ion conductor (LLZTO) particles at various temperatures. Selected PCEs with DEGDME additives, as model materials to investigate mechanism of σ_{dc} enhancement, were tested as well. The highest σ_{dc} at 30 °C detected in our testing is 1.3×10^{-3} S/cm in PEO_{18}-$LiClO_4$-10 wt% 500 nm-LLZTO-5 wt% DEGDME. It also exhibits good toughness (integrality and flexibility) and mechanical strength[11, 31] (G' > 1 MPa at 30 °C), as shown in Figure 2c and 2d. The membrane is in solid-state, confirmed by G' > G". With further increase of DEGDME content as depicted in Figure 2a, the σ_{dc} monotonically reduces. This trend qualitatively matches simulation results by the percolation theory.[15] The enlarged space of σ_{dc} alteration, depending on several control parameters, provides a foundation for analyzing mechanism of ion transport in PCEs.

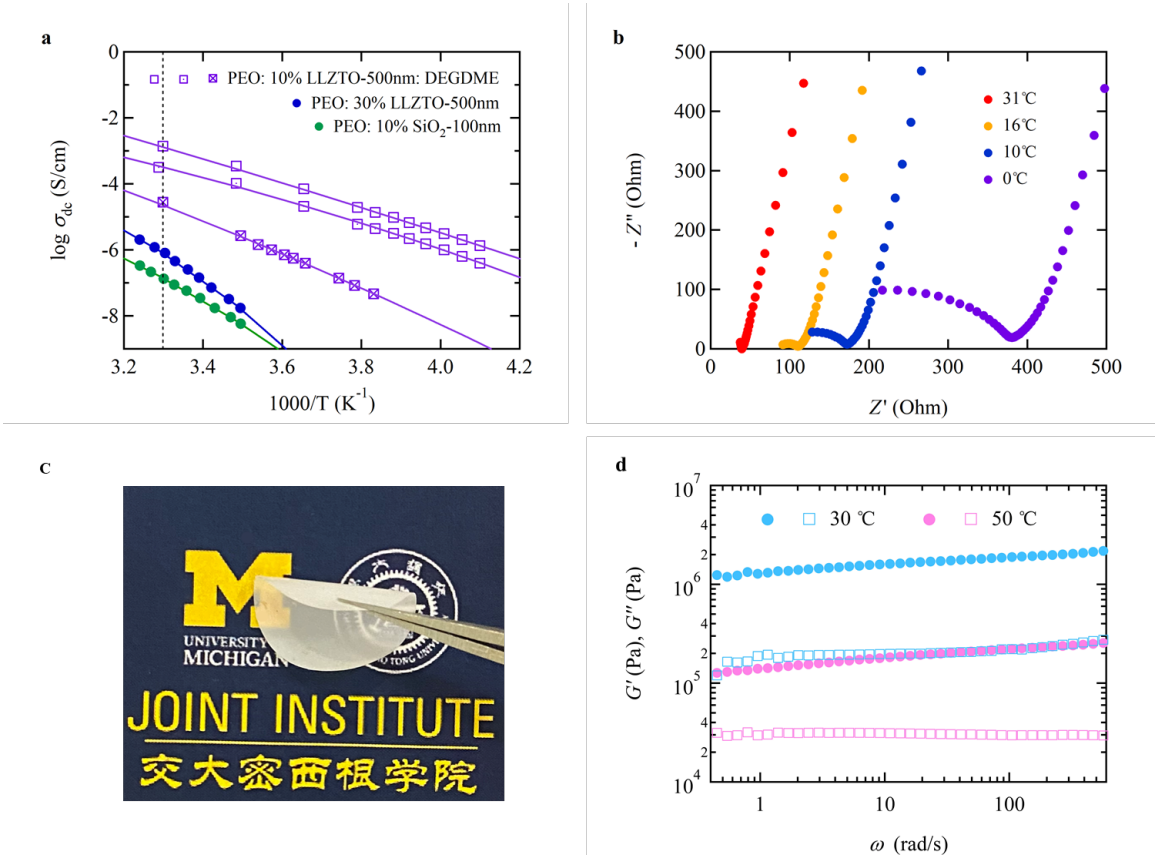

Figure 2. Ionic transport in selected samples. (a) Representative dc conductivity as a function of inverse temperature. Dash line indicates 30 °C. Symbols of ☐, ⊡ and ⊠ represent data from samples with increasing weight fraction of DEGDME. **(b)** Nyquist plots at various temperatures. **(c)** Photograph of a freestanding membrane shows flexibility. Sample: PEO_{18}-$LiClO_4$-10 wt% 500 nm-LLZTO-5 wt% DEGDME. **(d)** Shear modulus as a function of frequency of the sample in (c) at 30 and 50 ℃. Filled circles and open squares represent the storage modulus G' and loss modulus G", respectively.

To demonstrate the governing equations of ionic conductivity using parameters of dynamic relaxations, we further explore correlations between σ_{dc} and relaxation time (τ_{inter}, τ_{α}) or dielectric strength ($\Delta\varepsilon_{inter}$, $\Delta\varepsilon_{\alpha}$). Considering the fillers and the surrounding surface charge layer as two in-series layers, the characteristic time of MWS polarization is given by:[32]

$$\tau_{inter} \approx \tau_c \delta = \frac{\varepsilon_0 \varepsilon_s}{\sigma_{dc}} \delta \tag{1}$$

and

$$\delta = \frac{D_v}{2L_D} = \frac{\varepsilon_s}{\varepsilon_\infty} \tag{2}$$

where τ_c is the mean relaxation time for conductivity, D_v is the average diameter of particles, in this work obtained from 3D nano CT imaging (Figure S2-4), L_D is the Debye length.

Combing equation (1) and (2), we get

$$\log(\sigma_{dc}) = -\log(\tau_{inter}) + \log(\frac{\varepsilon_0 \varepsilon_s^{\,2}}{\varepsilon_\infty}) \tag{3}$$

In a similar form, σ_{dc} correlates with the α (or α_2) process:[33]

$$\log(\sigma_{dc}) = -\log(\tau_\alpha) + C \tag{4}$$

where C is a constant. Thus $1/\tau_\alpha$ can be considered as a measure of the velocity of ion dissociation. Figure 3 summarizes the influence of MWS and α relaxation on σ_{dc}. Equation (3) quantitatively describes the effect of τ_{inter} in most samples (Figure 3a), except for the data set of PEO_{18}-$LiClO_4$-5 μm-SiO_2 at low weight loadings. Similar trend is also found after adding of DEGDME (Figure S18). In these cases, τ_c values may show a distribution across the interface leading to a more complicated situation,[34] and hence τ_{inter} is no longer be proportional to τ_c. As shown in Figure 3a and 3b, plasticizer increases σ_{dc} by accelerating interfacial and segmental

dynamics, leading to a reduction of τ_{inter} and τ_{α}. In contrast, ceramic particles do not exhibit any clear trend on either increasing or decreasing relaxation times in these dynamic processes, compared with the particle-free PEO. The results suggest that the strategy of merely adding ceramic particles in PCEs has limited potential to substantially increase ionic conductivity.

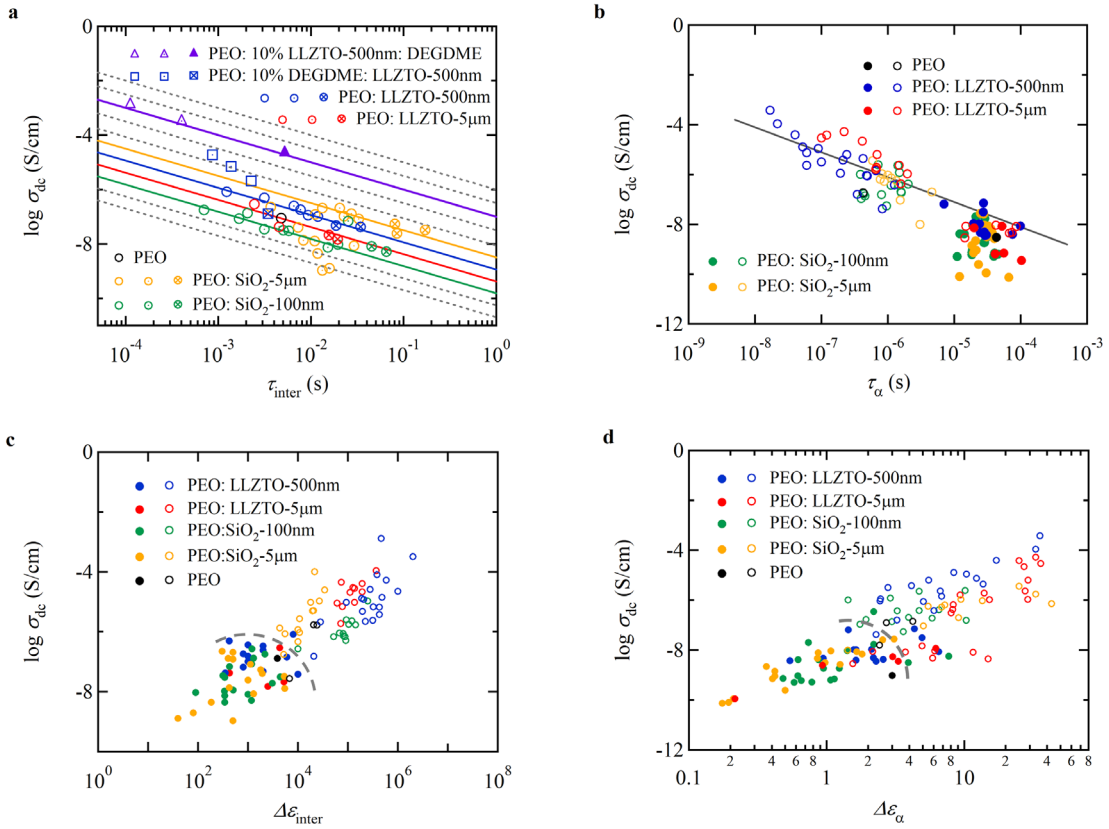

Figure 3. DC conductivity versus dynamic process parameters. (a) and **(c)** MWS process measured at T = 30 ℃. **(b)** and **(d)** α process measured at T = 17 ℃. All lines in (a) & (b) demonstrate the same slope of -1, obtained from Equation (3) or Equation (4). Symbols of □, ⊡ and ⊠, together with ○, ⊙ and ⊗ represent data from samples with increasing weight fraction of LLZTO particles. Symbols of △, ◬, and ▲ represent data from samples with increasing weight fraction of DEGDME. Closed and open symbols in (b)-(d) represent samples without and with DEGDME, respectively. Scattering of the same symbols reflects the results from various weight fractions of LLZTO particle and DEGDME plasticizer. The thick dash grey curve roughly indicates the boundary of open and closed data points, i.e., with or without DEGDME.

Figure 3c and 3d present similar alterations after DEGDME addition. Promoted $\Delta\varepsilon$ implies a higher concentration of ions participated in transport,[35, 36] which further leads to the increase of σ_{dc}. As limited by coordination number, that is, the number of oxygen atoms bonded with

Li^+, [37] magnitude of $\Delta\varepsilon_\alpha$ increase is far less than that of $\Delta\varepsilon_{inter}$ increase. Nevertheless, the number of sites for α relaxation taking place is expected to be much greater.

2.3 Mechanism for σ_{dc} improvement

We further analyze the microscopic origins for the σ_{dc} enhancement. The Li^+ conductivity can be expressed by:

$$\sigma_{dc} = p\mu q \tag{5}$$

where p is the concertation of mobile Li^+, μ is the Li^+ mobility, and q is the elementary charge. The Debye length, a measure of space charge layer thickness at interfaces, can be related to p and q by:[38]

$$L_D = \left(\frac{\varepsilon_s \varepsilon_0 k_B T}{q^2 p}\right)^{1/2} \tag{6}$$

where k_B is the Boltzmann constant, and T is the absolute temperature. From Equation (1), (2), (5), and (6), p, μ and L_D are determined by:

$$L_D = \left(\frac{\varepsilon_s \varepsilon_0 k_B T}{q^2 p}\right)^{1/2} \tag{7}$$

$$p = \frac{\varepsilon_s \varepsilon_0 k_B T}{q^2 L_D^{\,2}} \tag{8}$$

$$\mu = \frac{\sigma_{dc}}{pq} \tag{9}$$

and their effects on σ_{dc} are illustrated in Figure 4. These plots show consistent trends of σ_{dc} upon p, μ and L_D in all cases with and without DEGDME, suggesting a strategy for altering σ_{dc}. DEGDME markedly promotes σ_{dc} by increasing concentration of mobile Li^+ (Figure 4a) and reducing L_D at interfaces (Figure 4c), while Li^+ mobility, a measure of ion's ability to move through the PCE, mainly remains at the same level (Figure 4b). Ceramic particle-reinforced PCEs manifest higher p values, with or without the presence of plasticizer, compared with PCEs

filled by inert particles. Importantly, the plasticizer reduces activation energy (Figure 2a), releases a portion of inactive Li^+s to participate in ion transport, and thus apparently increases p, as illustrated in Figure 4a. Note that the dependence rates of σ_{dc} in Figure 4a and 4c in PCEs with DEGDME are roughly twofold of those in DEGDME-free samples, reflecting effects by accelerated dynamic processes. Combining experimental results above, increasing the density of active ions and simultaneously speeding up micro-dynamic processes for ion movement is an effective strategy for improving σ_{dc}.

From the results in Figure 3 and Figure 4, the effect of particle size on ionic transport is not notably recognized, whereas LLZTO particles demonstrate slightly better electrochemical performance than SiO_2, both well dispersed in PEO.

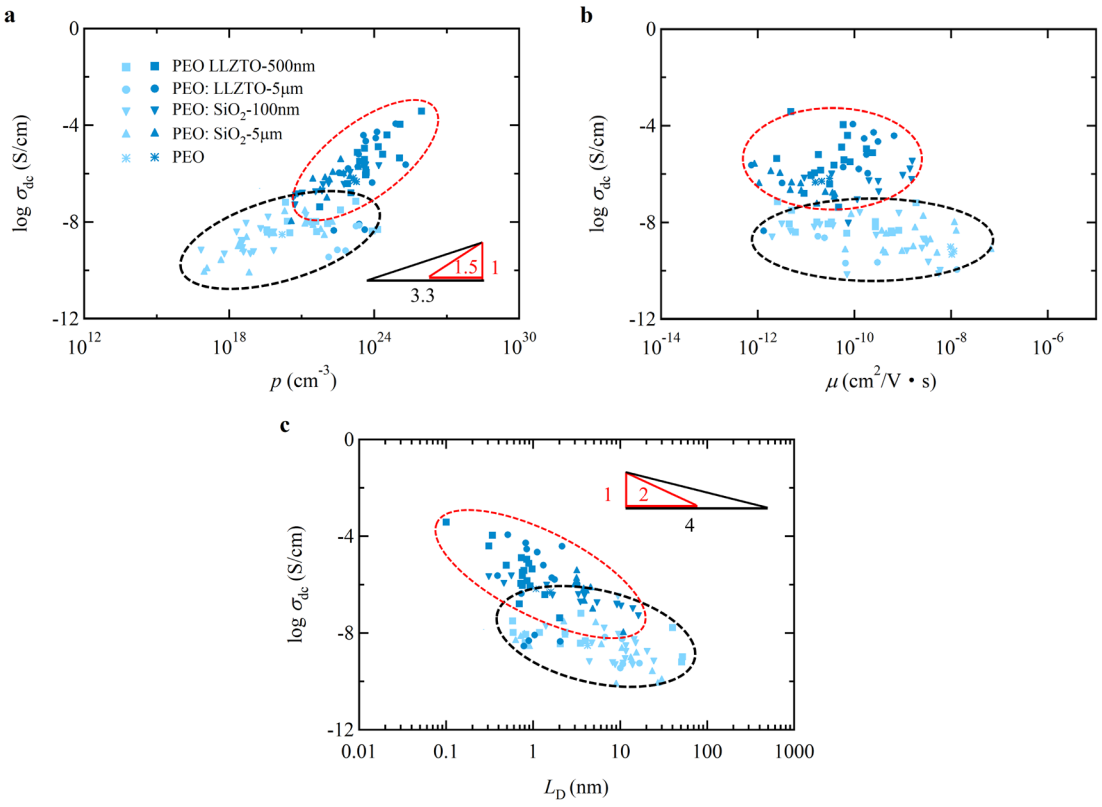

Figure 4. Conductivity dependence, on **(a)** ion concentration, **(b)** ion mobility and **(c)** Debye length, at $T = 17$ ℃.Black elliptical circles provide guides for the eye, on the range and trend of data from samples without plasticizer addition, whereas the red ellipses show the results from samples with plasticizer. Scattering of the same symbol reflects the results from various weight fractions of particles and DEGDME. The color ramps indicate relative rates in the dependence.

2.4 Coupling between relaxation processes

The MWS, α and α_2 processes show a similar dependence upon σ_{dc} with addition of small molecules. This inspires us to explore the interrelation between them. In thermorheologically simple materials, it is assumed that these sub-molecular relaxations manifest an identical temperature dependence, i.e., a change in temperature equally shifts the frequency of such relaxations to the same degree. However, this coupling manner does not work under some circumstances. For example, decoupling of chain relaxation from sub-molecular relaxation is detected and attributed to spatial heterogeneity which modifies local structural relaxation.[39] To analyze dynamic processes in PCEs, we adopt a decoupling degree, θ, as an exponent in the equation $\tau_{inter}T / \tau_{\alpha} = \tau_{inter}^{\theta}$, which is utilized to evaluate coupling between MWS and α processes. From results in Figure 4, evidently $\tau_{inter}T / \tau_{\alpha}$ vs. τ_{inter} results in a straight line in a double-logarithmic space, as all these variables display a linear dependence to σ_{dc} on a logarithmic scale. Figure 5a depicts coupling relations of representative samples, at various temperatures for each. With the addition of DEGDME, $\tau_{inter}T / \tau_{\alpha}$ exhibits a horizontal line (θ = 0) that indicates a strong coupling between interfacial dynamics and segmental relaxations in our temperature range. The neat PCE sample shows a linear dependence with a slope θ = 0.3, suggesting a less coupling under such circumstances. Figure 5b directly illustrates correlations between τ_{inter} and τ_{α} for a family of samples at 17 °C. Clearly, adding small molecules makes τ_{α} be proportional to τ_{inter}, whereas τ_{α} is proportional to $\tau_{inter}^{0.3}$ for plasticizer-free PCEs, in agreement with the results in Figure 5a. Therefore, the enhanced coupling between τ_{inter} and τ_{α}, together with a substantial shortening of these relaxation times, that rationalizes both α (including α_2, Figure S22) and MWS dynamics, are concurrently trigged and work in speeding up segmental and ionic motions on a microscopic scale.

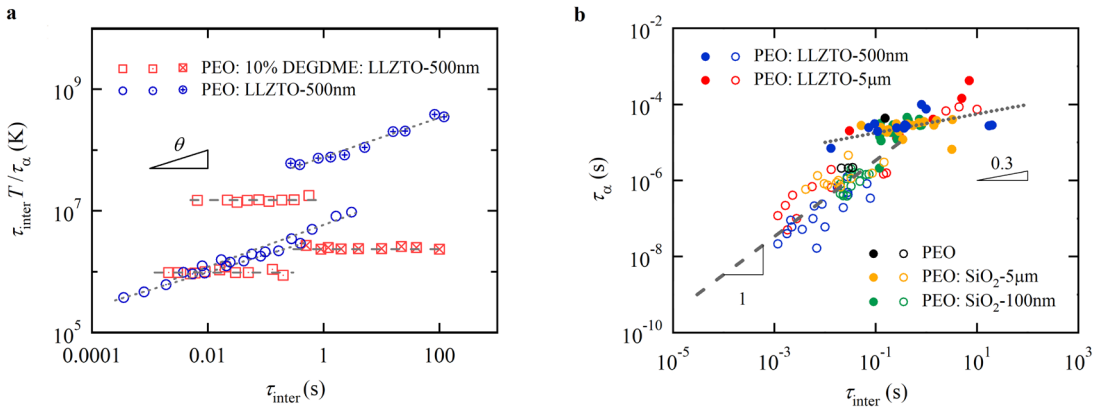

Figure 5. Coupling between α relaxation and MWS polarization. (a) $\tau_{inter} T / \tau_\alpha$ and **(b)** τ_α versus τ_{inter}. The closed and open circles represent samples without and with DEGDME. Symbols of □, ⊡ and ⊠; ○, ⊙ and ⊗ represent data from samples with increasing weight fraction of LLZTO particles. The decoupling degree θ in (a) for PEO: LLZTO-500nm is 0.3. Each data point in (a) represents the result from a single temperature. All data in (b) are measured at 17 ℃.

It is also worth noting that our results are in line with existing findings or consensuses in the literature. For instance, on of the effects of introducing ceramic particles is widely recognized as to suppress the crystallization of PEO, because amorphous phases majorly contribute to ionic conductivity.[2] Similar endeavors aiming to attain high-level ion dissociations have been made using block copolymers, wherein the short-chain PEO phases are dynamically active due to confinement by adjacent rigid phases from the other block. We found the crystallinities of PEO in our PCE samples remain at a narrow interval (Table S3 and S4, Figure S11), lower than the particle-free case, even though the weight loading of LLZTO varies in a broad range.[40] Moreover, we noted that the σ_{dc} in our samples varies in a manner quantitatively matching the percolation theory (Figure S10). Our results do not exhibit a clear trend of σ_{dc} change due to the particle size effect, yet it is reported that decreasing nanoparticle size diminishes interfacial effects in polymer-nanoparticle composites.[41]

3. Conclusions

In this paper, we demonstrated how dynamic processes quantatively determine ionic conductivity in solid PCEs, and elucidated the mechanism of improving ion transport, which

shows that accelerated polymer sub-chain dynamics, together with decreased charge-concentrated interfacial layer which releases more mobile ions, thus dedicates to σ_{dc} enhancement. The findings unveil principles of ion transport in multiphase composites, and offer valuable strategies for increasing σ_{dc} with an emphasis on speeding up segmental motion and interfacial polarization. It has been recently shown that establishing continuous interfaces along aligned ceramic nanowires effectively increases σ_{dc}.[16-18] The work further confirmed that the increase is originated from the interfacial ion pathways.

In summary, the ion transport mechanism revealed in this work may provide novel approaches for further improvement of ionic conductivity of solid PCEs at ambient temperature, besides keeping their merits ranging from thermal safety, solid yet flexible mechanical properties, and ease for commercial productions.

4. Material and Methods

Materials and Sample Fabrication. PEO was purchased from Sigma-Aldrich and was used without any further purification. The weight-average molecular weight of the PEO ($M_{W,PEO}$) is 600,000 g/mol. LLZTO particles with average diameters of 5 μm and 500 nm were purchased from Shanghai Kejing Precision Manufacturing. SiO_2 particles with diameter of 5 μm and 100 nm were purchased from Shanghai Aladdin Biochemical Technology. Different particle sizes were chosen to influence the pathway forming on polymer/particle interfaces. Fabrication procedure of the polymer-ceramic particle composite electrolytes composed of PEO_{18}-$LiClO_4$-*x* wt% LLZTO or SiO_2 is described previously.[40] Briefly, the PCE films were fabricated by blade coating and were subsequently dried by annealing at 50 ℃ under vacuum for 24 h. The thickness of resultant films is around 20-50 μm, depending on different compositions of samples. Distribution and an average size of particles or particle clusters were detected by nano CT imaging (Figure S2-5 and Table S1). In addition, a certain amount (5, 10, or 20 wt %) DEGMDE (purchased from Macklin Biochemical), was added to the mixture of PEO_{18}-$LiClO_4$-5 wt% LLZTO. The nominal weight percentages of LLZTO and SiO_2 particles were ascertained

by thermogravimetric analysis (Figure S6-7, Table S2).

Dielectric Relaxation Spectroscopy. DRS measurements were performed by using a Solartron Analyzer. A customized oven with an uncertainty of ± 0.5 ℃ from Shanghai Doaho was equipped for temperature control. The composite electrolytes were measured under an oscillating voltage of 100 mV in the frequency range from 1 MHz to 0.1 Hz at various temperatures. Electrolyte membrane with a diameter of 17 mm and thickness of 20-50 μm was sandwiched between two stainless steel blocking electrodes with a diameter of 16 mm to form a coin cell. The coin cell was firstly heated to an elevated temperature for 10 min to completely melt the PEO crystals, subsequently was quenched to 30 ℃. The DRS measurements were conducted right after 16 h at T_c to ensure full development of crystallization. The crystallization process was reported in our previous work.[40] It is worth noting that water absorption has a significant impact. It causes an unusual increase in ionic conductivity and the results were not reproducible after heat treatment. Hence, all of our samples were prepared in an argon glovebox. Measurements were carried right after annealing to avoid long-time storage in the glovebox. Samples after 24 h annealing treatment are proved no residual acetonitrile (2100-2400 cm^{-1}) and absorbed water by FTIR, as shown in Figure S8. We double checked if the samples contained any water after characterizations.

For PEO-based electrolytes, the dielectric response is dominated by charge carriers, i.e., the Ohmic conduction preponderates in dielectric spectra. It shows above glass transition temperature as a linear increase with decreasing frequency of the dielectric loss on a logarithmic scale:

$$\varepsilon_{\sigma}^{''}(\omega) = \frac{\sigma_{dc}}{\omega \varepsilon_0} \tag{10}$$

where ε_0 is dielectric permittivity of vacuum ($\varepsilon_0 = 8.854 \times 10^{-12}$ $V^{-1} \cdot m^{-1}$). Although it does not cover up the whole frequency range (see details in the *Supporting Information*), its contribution is considered a limiting factor as it may obscure loss peaks of dipole origin. Hence this effect

should be eliminated to elucidate high-frequency relaxation processes, by using the Kramers-Kronig relationship. The Ohmic-conduction free loss was thus determined from derivative of ε'_r:[42, 43]

$$\varepsilon_{der}''(\omega) = -\frac{\pi}{2}\frac{\partial \varepsilon_r''(\omega)}{\partial \ln \omega} \tag{11}$$

Wübbenhorst and co-workers[43] have shown that this method is a close approximation of the conduction-free loss in highly conductive systems.

Relaxation processes at high frequencies (α and α_2) were then analyzed by the Havriliak–Negami (HN) function:[44]

$$\varepsilon_{HN}^*(\omega) = \varepsilon_\infty + \frac{\Delta\varepsilon}{(1+(i\omega\tau_{HN})^a)^b} \tag{12}$$

where $\varepsilon_{HN}^*(\omega) = \varepsilon_r'(\omega) - i\varepsilon_r''(\omega)$, ω is angular frequency, and a and b are shape parameters satisfying constraints $0 < a$, and $ab \leq 1$, $\Delta\varepsilon = \varepsilon_s - \varepsilon_\infty$, ε_s and ε_∞ are the unrelaxed ($\omega = 0$) and relaxed ($\omega = \infty$) values of the dielectric permittivity, respectively. EP process is fitted by Debye model ($a = b = 1$ in Equation (12)).

Similarly, the MWS process at low frequencies was analyzed by an empirical modification of the Macdonald model:[45]

$$\varepsilon_{inter}^*(\omega) = \varepsilon_\infty + \frac{\Delta\varepsilon_{inter}}{(i\omega\tau_{inter})^{1-m} + i\omega\tau_{inter}} \tag{13}$$

where the subscript inter indicates the interfacial polarization, and $0 < m \leq 1$. Equation (13) is mathematically equivalent to a constant phase element-type equivalent circuit. We find it works fairly well in fitting MWS, with m determined to be 0.91~0.99. Note that inappropriate fitting may result in an unlimited increase of both real and imaginary permittivities at low frequencies,[46] since the imaginary part of permittivity is proportional to dissipation energy and vanishes when the real part approaches ε_s.

However, as the shape of the loss curve is very sensitive to the subtraction of dc conductivity,[47, 48] loss peaks appear much narrower in ε''_{der} than in ε''_{r}. Hence the derivative analysis should only be used to extract the relaxation time. The rest parameters ($\Delta\varepsilon$, ε_∞ and shape parameters a, b, m) are refined from the raw data $\varepsilon_r^*(\omega) = \varepsilon_r'(\omega) - i\varepsilon_r''(\omega)$, which are represented by the sum of individual processes:

$$\varepsilon_r^*(\omega) = \varepsilon_\infty + i\frac{\sigma_{dc}}{\omega\varepsilon_0} + \frac{\Delta\varepsilon_{inter}}{(i\omega\tau_{inter})^{1-m} + i\omega\tau_{inter}} + \sum_{EP,\alpha,\alpha_2} \frac{\Delta\varepsilon}{(1+(i\omega\tau_{HN})^a)^b} \quad (14)$$

The relaxation processes are rather narrow and symmetric, i.e., a varies from 0.86~0.95 and b = 1 in Equation (12) for segmental relaxations, MWS process described by Equation (13) is also close to the Debye model. The fact suggests low possibilities of process submerging one another and thus assures accuracy. Fitting example is shown in *Supporting Information.*

Supporting Information

Supporting Information is available from the Wiley Online Library or from the author.

Acknowledgements

The authors acknowledge the National Natural Science Foundation of China for financial support through the General Program 2157408.

References

[1]. Manthiram, A.; Yu, X.; Wang, S., Lithium battery chemistries enabled by solid-state electrolytes. *Nat. Rev. Mater.* **2017**, *2*, 16103.

[2]. Zhao, Q.; Stalin, S.; Zhao, C.-Z.; Archer, L. A., Designing solid-state electrolytes for safe, energy-dense batteries. *Nat. Rev. Mater.* **2020**, *5*, 229-252.

[3]. Kumar, B.; Scanlon, L. G., Polymer-ceramic composite electrolytes. *J. Power Sources* **1994**, *52*, 261-268.

[4]. Fergus, J. W., Ceramic and polymeric solid electrolytes for lithium-ion batteries. *J. Power Sources* **2010**, *195*, 4554-4569.

[5]. Pan, K.; Zhang, L.; Qian, W.; Wu, X.; Dong, K.; Zhang, H.; Zhang, S., A flexible ceramic/polymer hybrid solid electrolyte for solid-state lithium metal batteries. *Adv. Mater.* **2020**, *32*, 2000399.

[6]. Huo, H.; Chen, Y.; Luo, J.; Yang, X.; Guo, X.; Sun, X., Rational design of hierarchical "ceramic-in-polymer" and "polymer-in-ceramic" electrolytes for dendrite-free solid-state batteries. *Adv. Energy Mater.* **2019**, *9*, 1804004.

[7]. Tang, S.; Guo, W.; Fu, Y., Advances in composite polymer electrolytes for lithium batteries and beyond. *Adv. Energy Mater.* **2021**, *11*, 2000802.

[8]. Chen, L.; Li, Y.; Li, S.-P.; Fan, L.-Z.; Nan, C.-W.; Goodenough, J. B., PEO/garnet composite electrolytes for solid-state lithium batteries: From "ceramic-in-polymer" to "polymer-in-ceramic". *Nano Energy* **2018**, *46*, 176-184.

[9]. Nan, C. W.; Fan, L.; Lin, Y.; Cai, Q., Enhanced ionic conductivity of polymer electrolytes containing nanocomposite SiO2 particles. *Phys. Rev. Lett*. **2003**, *91*, 266104.

[10]. Srivastava, S.; Schaefer, J. L.; Yang, Z.; Tu, Z.; Archer, L. A., 25th anniversary article: polymer-particle composites: phase stability and applications in electrochemical energy storage. *Adv. Mater.* **2014**, *26*, 201-34.

[11]. Mackanic, D. G.; Yan, X.; Zhang, Q.; Matsuhisa, N.; Yu, Z.; Jiang, Y.; Manika, T.; Lopez, J.; Yan, H.; Liu, K.; Chen, X.; Cui, Y.; Bao, Z., Decoupling of mechanical properties and ionic conductivity in supramolecular lithium ion conductors. *Nat. Commun.* **2019**, *10*, 5384.

[12]. Dam, T.; Jena, S. S.; Pradhan, D. K., Coupled ion conduction mechanism and dielectric relaxation phenomenon in PEO20−LiCF3SO3‑based ion conducting polymer nanocomposite electrolytes. *J. Phys. Chem. C* 2018, *122*, 4133-4143.

[13]. Li, Z.; Huang, H.-M.; Zhu, J.-K.; Wu, J.-F.; Yang, H.; Wei, L.; Guo, X., Ionic conduction in composite polymer electrolytes: Case of PEO: Ga-LLZO composites. *Appl. Mater. Interfaces* **2019**, *11*, 784−791.

[14]. Yamada, H.; Bhattacharyya, A. J.; Maier, J., Extremely high silver ionic conductivity in composites of silver halide (AgBr, AgI) and mesoporous alumina. *Adv. Funct. Mater.* **2006**, *12*, 525–530.

[15]. Maier, J., Ionic conduction in space charge regions. *Prog. Solid St. Chem.* **1995**, *23*, 171-263.

[16]. Liu, W.; Lee, S. W.; Lin, D.; Shi, F.; Wang, S.; Sendek, A. D.; Cui, Y., Enhancing ionic conductivity in composite polymer electrolytes with well-aligned ceramic nanowires. *Nat. Energy* **2017**, *2*, 17035.

[17]. Liu, W.; Lin, D.; Sun, J.; Zhou, G.; Cui, Y., Improved lithium ionic conductivity in composite polymer electrolytes with oxide-ion conducting nanowires. *ACS Nano* **2016**, *10*, 11407-11413.

[18]. Liu, W.; Liu, N.; Sun, J.; Hsu, P.-C.; Lee, H.-W.; Cui, Y., Ionic conductivity enhancement of polymer electrolytes with ceramic nanowire fillers. *Nano Lett.* **2015**, *15*, 2740-2745.

[19]. Wan, J.; Xie, J.; Kong, X.; Liu, Z.; Liu, K.; Shi, F.; Pei, A.; Chen, H.; Chen, W.; Chen, J.; Zhang, X.; Zong, L.; Wang, J.; Chen, L.-Q.; Qin, J.; Cui, Y., Ultrathin, flexible, solid polymer composite electrolyte enabled with aligned nanoporous host for lithium batteries. *Nat. Nanotechnol.* **2019**, *14*, 705-711.

[20]. Bouchet, R. M., S.; Meziane, R.; Aboulaich, A.; Lienafa, L.; Bonnet, J.-P.; Phan, T. N. T.; Bertin, D.; Gigmes, D.; Devaux, D.; Denoyel, R.; Armand, M., Single-ion BAB triblock copolymers as highly efficient electrolytes for lithium-metal batteries. *Nat. Mater.* **2013**, *12*, 452-457.

[21]. Morris, M. A.; Sung, S. H.; Ketkar, P. M.; Dura, J. A.; Nieuwendaal, R. C.; Epps III, T. H., Enhanced conductivity via homopolymer-rich pathways in block polymer-blended electrolytes. *Macromolecules* **2019**, *52*, 9682-9692.

[22]. Nakamura, I.; Balsara, N. P.; Wang, Z. G., Thermodynamics of ion-containing polymer blends and block copolymers. *Phys Rev Lett* **2011**, *107*, 198301.

[23]. Lu, Q.; He, Y.-B.; Yu, Q.; Li, B.; Kaneti, Y. V.; Yao, Y.; Kang, F.; Yang, Q.-H., Dendrite-free, high-rate, long-Life lithium metal batteries with a 3D cross-linked network polymer electrolyte. *Adv. Mater.* **2017**, *29*, 1604460.

[24]. Shin, D.-M.; Bachman, J. E.; Taylor, M. K.; Kamcev, J.; Park, J. G.; Ziebel, M. E.; Velasquez, E.; Narenwattananon, N. N.; Sethi, G. K.; Cui, Y.; Long, J. R., A single-ion conducting borate network polymer as a viable quasi-solid electrolyte for lithium metal batteries. *Adv. Mater.* **2020**, *32*, 1905771.

[25]. Das, S.; Ghosh, A., Charge carrier relaxation in different plasticized PEO/PVDF-HFP blend solid polymer electrolytes. *J. Phys. Chem. B* **2017**, *121*, 5422-5432.

[26]. Tu, Z.; Zachman, M. J.; Choudhury, S.; Wei, S.; Ma, L.; Yang, Y.; Kourkoutis, L. F.; Archer, L. A., Nanoporous hybrid electrolytes for high-energy batteries based on reactive metal anodes. *Adv. Energy Mater.* **2017**, *7*, 1602367.

[27]. Paulsdorf, J.; Kaskhedikar, N.; Burjanadze, M.; Obeidi, S.; Stolwijk, N. A.; Wilmer, D.; Wiemhöfer, H.-D., Synthesis and ionic conductivity of polymer electrolytes based on a polyphosphazene with short side Groups. *Chem. Mater.* **2006**, *18*, 1281-1288.

[28]. Choi, U. H.; Colby, R. H., The role of solvating 12-crown‑4 plasticizer on dielectric constant and ion conduction of poly(ethylene oxide) single-ion conductors. *Macromolecules* **2017**, *50*, 5582-5591.

[29]. Kobayashi, K.; Pagot, G.; Vezzù, K.; Bertasi, F.; Noto, V. D.; Tominaga, Y., Effect of plasticizer on the ion-conductive and dielectric behavior of poly(ethylene carbonate)-based Li electrolytes. *Polymer* **2020**, *53*, 149–155.

[30]. Brogioli, D.; Langer, F.; Kun, R.; Mantia, F. L., Space-Charge effects at the Li7La3Zr2O12/poly(ethylene oxide) interface. *ACS Appl. Mater. Interfaces* **2019**, *11*, 11999-12007

[31]. Choudhury, S.; Mangal, R.; Agrawal, A.; Archer, L. A., A highly reversible room-temperature lithium metal battery based on crosslinked hairy nanoparticles. *Nat. Commun.* **2015**, *6*, 10101.

[32]. Kremer, F.; Schönhals, A.; Lunkenheimer, P.; Loidl, A.; Huwe, A.; Różański, S. A.; Floudas, G.; Mijovic, J.; Hartmann, L.; Fukao, K.; Steeman, P. A. M.; Turnhout, J. v.; Böhmer, R.; Diezemann, G.; Richert, R.; Pakula, T.; A.Arbe; Colmenero, J.; Richter, D., Broadband dielectric spectroscopy. 1st ed.; Springer-Verlag Berlin Heidelberg: New York, 2003.

[33]. Walden, P., Organic solutions and ionisation means. III. chapter: internal friction and its connection with conductivity. *Phys. Chem.* **1906**, *55*, 249-257.

[34]. Lestrieza, B.; Maazouza, A.; Gerarda, J. F.; Sautereaua, H.; Boiteuxb, G.; Seytreb, G.; Kranbuehl, D. E., Is the Maxwell–Sillars–Wagner model reliable for describing the dielectric properties of a core–shell particle–epoxy system? *Polymer* **1998**, *39*, 6733–6742.

[35]. Wheatle, B. K.; Keith, J. R.; Mogurampelly, S.; Lynd, N. A.; Ganesan, V., Influence of dielectric constant on ionic transport in polyether-based electrolytes. *ACS Macro. Lett.* **2017**, *6*, 1362−1367.

[36]. Wheatle, B. K.; Lynd, N. A.; Ganesan, V., Effect of polymer polarity on ion transport: a competition between ion aggregation and polymer segmental dynamics. *ACS Macro. Lett*. **2018**, *7*, 1149−1154.

[37]. Das, D.; Chandrasekaran, A.; Venkatram, S.; Ramprasad, R., Effect of crystallinity on Li adsorption in polyethylene oxide. *Chem. Mater*. **2018**, *30*, 8804−8810.

[38]. Fragiadakis, D.; Dou, S.; Colby, R. H.; Runt, J., Molecular mobility, ion mobility, and mobile ion concentration in poly(ethylene oxide)-based polyurethane ionomers. *Macromolecules* **2008**, *41*, 5723-5728.

[39]. Sokolov, A. P.; Schweizer, K. S., Resolving the mystery of the chain friction mechanism in polymer liquids. *Phys. Rev. Lett*. **2009**, *102*, 248301.

[40]. Huang, Y.; Ma, M.; Guo, Y., Melt crystallization and segmental dynamics of poly(ethylene oxide) confined in a solid electrolyte composite. *J polym Sci* **2020**, *58*, 466–477.

[41]. Emamy, H.; Kumar, S. K.; Starr, F. W., Diminishing interfacial effects with decreasing nanoparticle size in polymer-nanoparticle composites. *Phys. Rev. Lett.* **2018**, *121*, 207801.

[42]. van Turnhout, J.; Wübbenhorst, M., Analysis of complex dielectric spectra. II: Evaluation of the activation energy landscape by differential sampling. *J. Non-Cryst. Solids* **2002**, *305*, 50-58.

[43]. Wübbenhorst, M.; van Turnhout, J., Analysis of complex dielectric spectra. I. One-dimensional derivative techniques and three-dimensional modelling. *J of Non-Crystalline Solids* **2002**, *305*, 40-49.

[44]. Havriliak, S.; Negami, S., A complex plane analysis of α-dispersions in some polymer systems. *J. Polym. Sci. C* **1966**, *14*, 99-117.

[45]. Brug, G. J.; Eeden, A. L. G. V. D.; Sluters-Rehbach, M.; Sluyters, J. H., The analysis of electrode impedances complicated by the presence of a constant phase element. *J. Electroanal Chem.* **1984**, *176*, 275-295.

[46]. Sarensen, T. S.; Cornpafib, V.; Diaz-Calleja, R., Complex permittivity of a film of poly [4-(acryloxy)phenyl= (4=chlorophenyl)methanone] containing free ion impurities and the separation of the contributions from interfacial polarization, Maxwell-Wagner-Sillars effects and dielectric relaxations of the polymer chains. *J. Chem. SOC., Faraday Trans.* **1996**, *92*, 1947- 1957.

[47]. MacKinnon, A. J.; Jenkins, S. D.; MacGrail, P. T.; Pethrick, R. A., Dielectric, mechanical and rheological studies of phase separation and cure of a thermoplastic modified epoxy resin: incorporation of reactively terminated polysulfones. *Polymer* **1993**, *34*, 3252-3263.

[48]. MacKinnon, A. J.; Jenkins, S. D.; MacGrail, P. T.; Pethrick, R. A., A Dielectric, mechanical, rheological, and electron microscopy study of cure and properties of a thermoplastic-modified epoxy resin. *Macromolecules* **1992**, *25*, 3492-3499.

TOC Figure

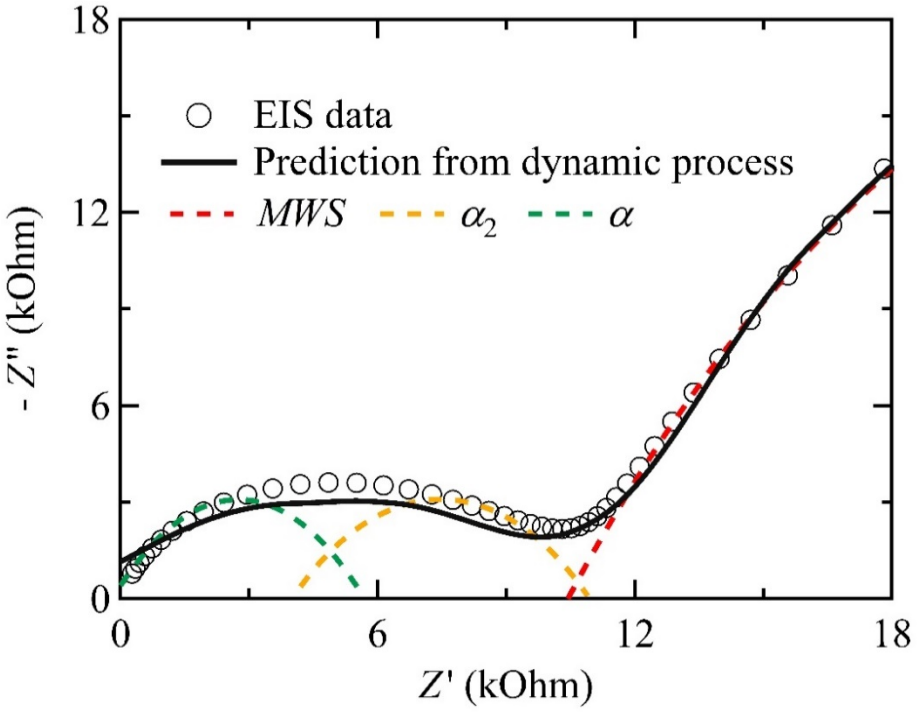

Caption: In solid polymer-ceramic composite electrolytes (PCEs), segmental motion and interfacial polarization turn to be directly coupled, both quantitively determine ion transport in PCEs. With small molecule additives, the solid composite electrolyte can achieve an ionic conductivity of 1.3×10^{-3} S/cm at 30 °C with moderate mechanical strength and toughness.

ToC Figure

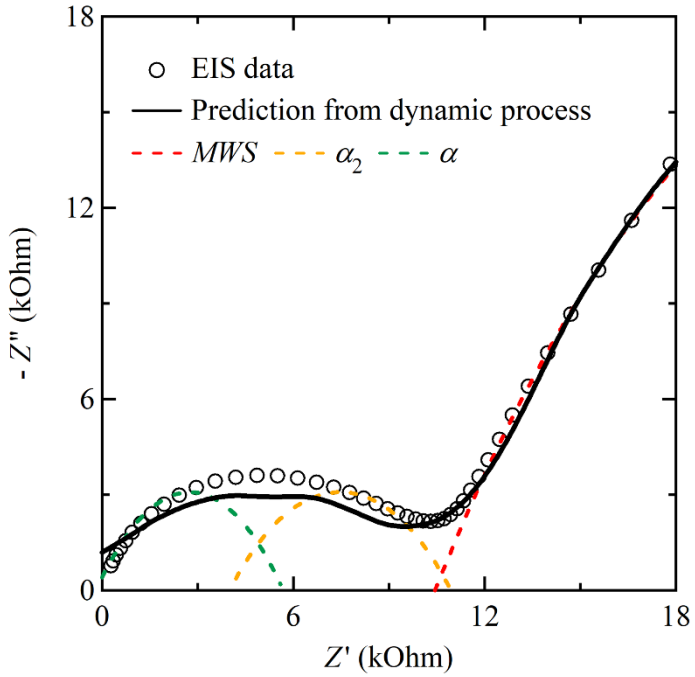

Caption: In solid polymer-ceramic composite electrolytes (PCEs), segmental motion and interfacial polarization turn to be directly coupled, both quantitively determine ion transport in PCEs. With small molecule additives, the solid composite electrolyte can achieve an ionic conductivity of 1.3×10^{-3} S/cm at 30 °C with moderate mechanical strength and toughness.